applied optics

Internal stray radiation measurement for cryogenic infrared imaging systems using a spherical mirror

Qijie Tian,[1,2,*] Songtao Chang,[1] Fengyun He,[1] Zhou Li,[1,2] and Yanfeng Qiao[1]

[1]Changchun Institute of Optics, Fine Mechanics and Physics, Chinese Academy of Sciences, Changchun, Jilin 130033, China
[2]University of Chinese Academy of Sciences, Beijing 100049, China
*Corresponding author: tian7jie@163.com

Received 14 March 2017; revised 15 May 2017; accepted 15 May 2017; posted 16 May 2017 (Doc. ID 290633); published 6 June 2017

Internal stray radiation is a key factor that influences infrared imaging systems, and its suppression level is an important criterion to evaluate system performance, especially for cryogenic infrared imaging systems, which are highly sensitive to thermal sources. In order to achieve accurate measurement for internal stray radiation, an approach is proposed, which is based on radiometric calibration using a spherical mirror. First of all, the theory of spherical mirror design is introduced. Then, the calibration formula considering the integration time is presented. Following this, the details regarding the measurement method are presented. By placing a spherical mirror in front of the infrared detector, the influence of internal factors of the detector on system output can be obtained. According to the calibration results of the infrared imaging system, the output caused by internal stray radiation can be acquired. Finally, several experiments are performed in a chamber with controllable inside temperatures to validate the theory proposed in this paper. Experimental results show that the measurement results are in good accordance with the theoretical analysis, and demonstrate that the proposed theories are valid and can be employed in practical applications. The proposed method can achieve accurate measurement for internal stray radiation at arbitrary integration time and ambient temperatures. The measurement result can be used to evaluate whether the suppression level meets the system requirement.

OCIS codes: (120.5630) Radiometry; (290.2648) Stray light; (110.3080) Infrared imaging; (040.2480) FLIR, forward-looking infrared.

https://doi.org/10.1364/AO.56.004918

1. INTRODUCTION

Stray radiation denotes the undesired radiation that reaches the image plane. It can degrade the image quality, affect system directivity, and reduce the signal-to-noise ratio (SNR) of a system [1–4]. For visible imaging systems, only the external stray light is necessary to be analyzed and suppressed, whereas, for infrared imaging systems, the self-radiation of a system, namely the internal stray radiation, must be considered and suppressed as well [5]. With the increasing requirement for high-performance infrared imaging systems, the stray radiation suppression level may dominate system performance [6]. Consequently, efficient control of stray radiation is required for all imaging systems. In order to detect small temperature differences, high-sensitivity infrared imaging systems generally employ cryogenic infrared detectors, which are extremely sensitive to thermal sources. Therefore, the internal stray radiation will have a significant influence on system performance. In order to evaluate whether the suppression level meets the system requirement or to guide the suppression design, the flux and the system output due to stray radiation must be quantified. However, the internal stray radiation measurement has attracted few investigations.

A number of methods have been put forward to achieve measurement of internal stray radiation. Nevertheless, those methods can be briefly divided into two categories. (1) With the development of computer technology, many programs and calculation methods have been developed to analyze internal stray radiation quantitatively by simulation. Typical methods are the ray-tracing method, Monte Carlo method, etc., [7–9]. The programs are TracePro, FRED, Lighttools, ASAP, and so on [10–12]. The simulation method does not need experimental conditions and is low cost. However, it has a significant drawback in that the simulation result may lead to huge errors, due to the deviations from the optical and mechanical geometry, as well as the optical properties. (2) When the system has been finished, the stray radiation suppression performance must be tested [13–16], whereas, for infrared imaging systems, the measurement result contains both internal and external stray radiation, which means we are

unable to obtain the internal stray radiation alone. Besides, expensive and complicated equipment is required to perform the measurement.

To overcome those drawbacks, some methods have been put forward. For example, Tian *et al.* [17] performed the radiometric calibration at two ambient temperatures to acquire the quantitative relation between the ambient temperature and the internal stray radiation. Then the internal stray radiation at various ambient temperatures can be calculated instead of conducting the measurement frequently. However, its drawback lies in the fact that it is hard to control large-aperture infrared imaging systems at two ambient temperatures, which means this method is inapplicable for large-aperture infrared systems. Chang *et al.* [18] calibrated the infrared detector to remove the influence of internal factors of infrared detectors on system output. By combing the calibration result of the infrared system at an integration time, the internal stray radiation can be acquired, whereas, the internal factors of the infrared detector will change as time goes on. As a result, the detector must be disassembled from the whole system and calibrated periodically to maintain measurement precision, which may result in high cost. In addition, the residual scatter of blackbody will lead to a measurement error for the detector internal factors.

In this paper, we propose a method to achieve the measurement of internal stray radiation of cryogenic infrared imaging systems using a spherical mirror. A short outline is presented as follows: in Section 2, the theory concerning the spherical mirror design is introduced. In Section 3, the calibration formula is deduced considering the integration time, and the details with regard to the measurement method are presented. Several experiments are performed to verify the theory described above in Section 4. The conclusion is given in Section 5.

2. SPHERICAL MIRROR DESIGN

The fundamental principle of the spherical mirror design is to prevent external thermal radiation from directly reaching the infrared focal plane array (IRFPA). According to the reversibility principle of ray path, all the rays traced from the IRFPA are completely reflected back to the cryogenic dewar by the spherical mirror. Meanwhile, the reflecting surface is polished and coated with high-reflection film, which has extraordinarily low emissivity.

The pertinent parameters required for the spherical mirror design are shown in Fig. 1. The x axis denotes the optical axis and the IRFPA is located at the point O(0,0), which is the origin of the coordinate. The radius and height of the spherical mirror are denoted as R and H, respectively. L denotes the distance from the reflecting surface to the IRFPA, $O_i(x_i, 0)$ is the coordinate of the center of the spherical mirror, l denotes the length of the cryogenic dewar, b is the semidiameter of the entrance pupil of the detector, and a denotes the half-length of the detector diagonal line.

The aim is to obtain the radius R and the height H of the spherical mirror. Because of the rotational symmetry of optical systems, only the detector diagonal line is considered during the whole analysis process. Furthermore, we only need to analyze the rays propagating to the $-y$ direction, and the rays

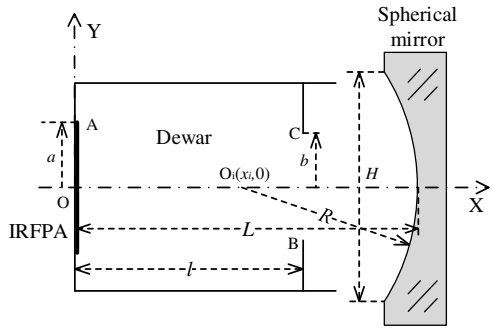

Fig. 1. Optical layout defining parameters of spherical mirror.

propagating to the $+y$ direction are similar due to the axial symmetry of the detector diagonal line. The critical rays that determine the spherical mirror range are ray AB and ray AC. The quadratic equation of the spherical mirror is given by

$$[x - (L - R)]^2 + y^2 = R^2. \tag{1}$$

As shown in Fig. 2, the critical ray AB originates from the positive edge of the detector diagonal line and passes at the negative edge of the entrance pupil. It strikes at $Q(x_B, y_B)$ on the reflecting surface, and after reflection it goes back in the same way it propagates outwards. The critical ray AB can be expressed in the form of a straight line equation as

$$y = k_1 \cdot x + b_1, \tag{2}$$

where $k_1 = -(a + b)/l$ and $b_1 = a$.

According to the law of reflection, the center of a spherical mirror is located at the intersection point of the critical ray AB and the optical axis, namely the zero point of Eq. (2). The maximum radius is denoted by $R_{\max}$ and can be obtained by Eq. (2). The minimum height, denoted as $H_{\min}$, equals to $|2y_B|$ and can be obtained by substituting Eq. (2) into Eq. (1).

The critical ray AC originates from the positive edge of the detector diagonal line and goes through the positive edge of the entrance pupil. It intersects at $P(x_C, y_C)$ on the reflecting surface. After reflection, it passes through the negative edge of the entrance pupil, as shown in Fig. 3. The critical ray AC can be written in the form of a straight line equation as

$$y = k_2 \cdot x + b_2, \tag{3}$$

where $k_2 = (b - a)/l$ and $b_2 = a$.

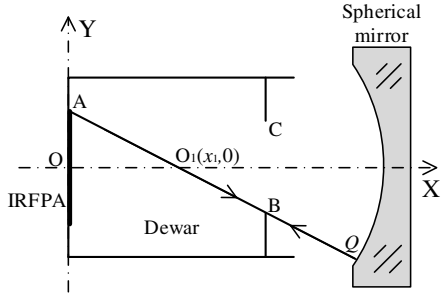

Fig. 2. Optical layout of the critical ray AB.

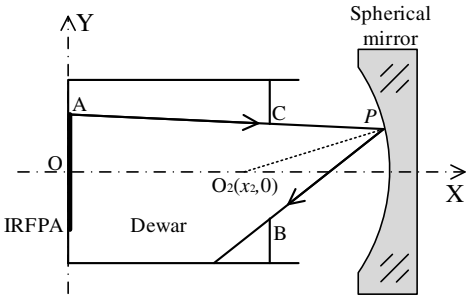

Fig. 3. Optical layout of the critical ray AC.

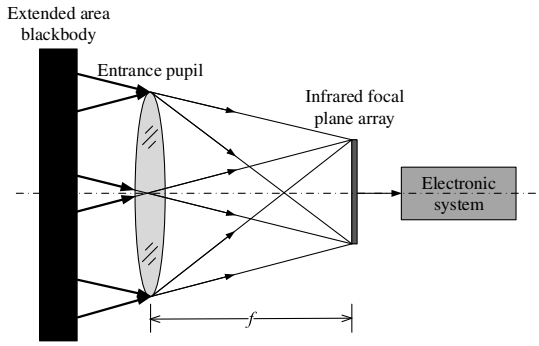

Fig. 4. Schematic of near-extended-source method.

The reflected ray PB can be written in the linear form as

$$y = k_3 \cdot x + b_3, \tag{4}$$

where $k_3 = (y_C + b)/(x_C - l)$ and $b_3 = -l \cdot (y_C + b)/(x_C - l) - b$.

The center of the spherical mirror is assumed to locate at point $O_2(x_2, 0)$, which can be acquired by

$$\frac{|k_3 \cdot x_2 + b_3|}{\sqrt{k_3^2 + 1}} = \frac{|k_2 \cdot x_2 + b_2|}{\sqrt{k_2^2 + 1}}. \tag{5}$$

The minimum radius is denoted by $R_{\min}$ and can be obtained by submitting $O_2(x_2, 0)$ to Eq. (1).

For now, we have acquired the parameter range of the spherical mirror, which can be expressed as

$$\left.\begin{array}{l} R \le R_{\max} \\ R \ge R_{\min} \\ H \ge H_{\min} \end{array}\right\}. \tag{6}$$

As shown in Fig. 1, the spherical mirror is placed at the position where it is L away from the IRFPA. The distance between the spherical mirror and the IRFPA should be appropriate considering the characteristics of optics and the detector, not too long or too close. Theoretically, external thermal radiation cannot directly reach the IRFPA, as long as R is in range $[R_{\min}, R_{\max}]$. In practical applications, we recommend choosing the median value as the radius value in consideration of the alignment error. When the radius R is determined, the minimum height $H_{\min}$ can be calculated according to Eq. (1). In summary, if Eq. (6) is satisfied, external thermal radiation cannot reach the IRFPA. Moreover, the self-radiation of the spherical mirror is extremely low, which can be ignored.

3. THEORY OF INTERNAL STRAY RADIATION MEASUREMENT

In order to acquire the response and offset of the infrared imaging system, the radiometric calibration must be conducted. Besides, a spherical mirror is required to remove the influence of internal factors of infrared detector on system output. In this section, the calibration model considering the integration time is deduced, and the details with regard to the proposed measurement method are presented.

A. Radiometric Calibration Considering the Integration Time

In this paper, the near-extended-source method is employed to achieve the radiometric calibration, as shown in Fig. 4. The blackbody, namely the reference source, is put close to the optics and covers the field of view (FOV) and the aperture of optics. As a result, the atmospheric effect can be ignored [19].

To achieve high dynamic range imaging as well as radiometric applications, typical infrared imaging systems are generally calibrated at several integration times [20,21]. The system output exhibits a linear relation to the incident radiance and the integration time within the linear response range of a cryogenic infrared detector. The linear relation at a preselected integration time can be expressed as [22]

$$\begin{aligned} h(t, T_{\text{amb}}) &= G \cdot L_t + B \\ &= t \cdot G_0 \cdot L_t + h_{\text{stray}}(t, T_{\text{amb}}) + h_{\text{det}}(t), \end{aligned} \tag{7}$$

where G is the response of a detector pixel on the IRFPA; B denotes the offset, which is caused by the self-radiation of the infrared optical system, namely, the internal stray radiation and the internal factors of cryogenic infrared detector such as the dark current; t is the integration time in units of ms; G_0 is the response of a detector pixel at unit integration time; $h_{\text{stray}}(t, T_{\text{amb}})$ denotes the output gray value caused by internal stray radiation at a given integration time under the ambient temperature T_{amb}; $h_{\text{det}}(t)$ refers to the internal factors of the cryogenic infrared detector at the given integration time. L_t denotes the incident radiance of the reference source, and can be obtained by [23]

$$L_t = \varepsilon \cdot L(T_t) = \frac{\varepsilon}{\pi} \int_{\lambda_1}^{\lambda_2} M(\lambda, T_t) \mathrm{d}\lambda, \tag{8}$$

where $L(T_t)$ is the radiance of an ideal blackbody at the temperature T_t, ε is the emissivity of the reference source, $M(\lambda, T_t)$ is the spectral radiant excitance calculated by Planck's formula, $\lambda_1 \sim \lambda_2$ is the integration spectral range. For a detector pixel on the IRFPA, the incident radiation flux that it receives can be calculated by [24]

$$\Phi_t = \frac{\pi \cdot \varepsilon \cdot \tau}{4} \cdot \left(\frac{D}{f}\right)^2 \cdot A_d \cdot L(T_t) = K_t \cdot L(T_t), \tag{9}$$

where τ is the transmissivity of optics, A_d is the detector pixel area, D is the diameter of optics, and f is the focal length of optics. As a result, the response of a detector pixel to the incident radiation flux can be written as $G' = G/K_t$.

B. Method to Measure Internal Stray Radiation

According to Eq. (7), the output gray value caused by internal stray radiation can be calculated by

$$h_{\text{stray}}(t, T_{\text{amb}}) = B - h_{\text{det}}(t). \tag{10}$$

Equation (10) implies that if the internal factors of the infrared detector are known, the output gray value caused by internal stray radiation can be acquired. The internal factors of the infrared detector are mainly caused by various kinds of noises, such as the dark current. Experiments have demonstrated that the internal factors have a linear connection with the integration time within the linear response range, which can be expressed as [18]

$$h_{\text{det}}(t) = t \cdot h_{\text{det1}} + h_{\text{det2}}, \tag{11}$$

where h_{det1} denotes the noise that has a linear connection with the integration time, and h_{det2} refers to the noise that is independent of the integration time.

In order to acquire the internal factors, the spherical mirror designed above is positioned in front of the infrared detector at the right position, as shown in Fig. 5. According to the fundamental principle of the spherical mirror design, we can learn that external thermal radiation cannot reach the IRFPA right now. Furthermore, the self-radiation of the spherical mirror is extremely low and can be ignored. Therefore, the detector output now is the internal factors.

Assume that the infrared detector has collected two infrared images at two different integration times, namely t_1 and t_2. The detector output can be presented as follows:

$$h_{\text{det}}(t_1) = t_1 \cdot h_{\text{det1}} + h_{\text{det2}}, \tag{12}$$

$$h_{\text{det}}(t_2) = t_2 \cdot h_{\text{det1}} + h_{\text{det2}}. \tag{13}$$

Thereupon, the internal factors can be calculated by Eqs. (12) and (13), which can be expressed as

$$h_{\text{det1}} = \frac{h_{\text{det}}(t_2) - h_{\text{det}}(t_1)}{t_2 - t_1}, \tag{14}$$

$$h_{\text{det2}} = \frac{h_{\text{det}}(t_1) \cdot t_2 - h_{\text{det}}(t_2) \cdot t_1}{t_2 - t_1}. \tag{15}$$

By substituting Eqs. (14) and (15) into Eq. (10), the output gray value caused by internal stray radiation at an arbitrary integration time and ambient temperatures, namely $h_{\text{det}}(t, T_{\text{amb}})$, can be calculated by

$$\begin{aligned} h_{\text{stray}}(t, T_{\text{amb}}) &= B - t \cdot h_{\text{det1}} - h_{\text{det2}} \\ &= B - t \cdot \frac{h_{\text{det}}(t_2) - h_{\text{det}}(t_1)}{t_2 - t_1} \\ &\quad - \frac{h_{\text{det}}(t_1) \cdot t_2 - h_{\text{det}}(t_2) \cdot t_1}{t_2 - t_1}. \end{aligned} \tag{16}$$

As shown in Eq. (16), the output gray value caused by internal stray radiation is in linear connection with the integration time when the ambient temperature is constant. According to Eq. (9), the flux resulting from internal stray radiation can be expressed as

$$\Phi_{\text{stray}}(T_{\text{amb}}) = \frac{h_{\text{stray}}(t, T_{\text{amb}})}{G'} = \frac{K_t}{t \cdot G_0} \cdot h_{\text{stray}}(t, T_{\text{amb}}), \tag{17}$$

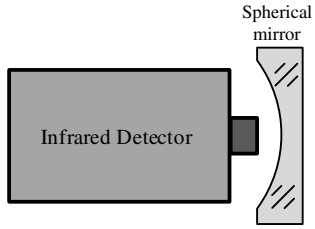

Fig. 5. Schematic of acquiring internal factors of infrared detector.

where $\Phi_{\text{stray}}(T_{\text{amb}})$ denotes the flux due to the internal stray radiation.

Equation (17) exhibits that for a given infrared imaging system, the flux originating from internal stray radiation is a function of the ambient temperature and independent of the integration time. Besides, the internal stray radiation flux is directly proportional to the radiance of an ideal blackbody at the ambient temperature, and can be presented as [25]

$$\Phi_{\text{stray}}(T_{\text{amb}}) = K_{\text{stray}} \cdot L(T_{\text{amb}}). \tag{18}$$

The system output and flux resulting from internal stray radiation at arbitrary ambient temperatures and integration time can be acquired according to Eqs. (16) and (17). When the measurement is performed, the spherical mirror designed above is placed in front of the detector at the right position, and the influence of internal factors of the infrared detector on system output can be acquired. Then only a general radiometric calibration is required to obtain the internal stray radiation. The proposed approach has many advantages, such as low demand for experimental conditions, ease of implementation and easy adoption by any cryogenic infrared imaging system. The measurement result can be used to evaluate whether the internal stray radiation suppression level meets the system requirement. Furthermore, the approach can be adopted to monitor the internal stray radiation in real time to detect surface contamination, structural distortion, or heat.

4. EXPERIMENTAL RESULTS AND ANALYSIS

A. Experimental Setup

To validate the theories introduced above experimentally, several experiments have been carried out with a mid-wave infrared (MWIR) optical system. The focal length of the MWIR optical system is 100 mm, and the aperture is 50 mm. The cryogenic MWIR detector manufactured by forward-looking infrared (FLIR) systems operates in a 3.7–4.8 μm wave band with a 14-bit digital output. And the IRFPA has a large scale of 640 pixels × 512 pixels, with an output noise of about 20 DN. The extended area blackbody of SR-800-4A, which is manufactured by CI systems, has a size of 100 mm × 100 mm and exhibits a high effective emissivity about 0.97 over the wave band from 3.7 to 4.8 μm. Its temperature accuracy can be controlled within ±0.01°C over the operating temperature range from 0°C to 125°C.

B. Internal Factors Measurement for MWIR Detector

In order to measure internal stray radiation, the internal factors of the cooled MWIR detector must be acquired. The

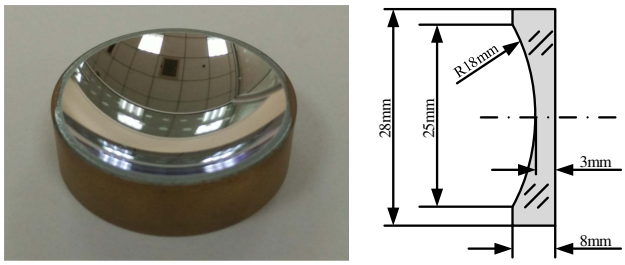

Fig. 6. Photo and parameter of the designed spherical mirror.

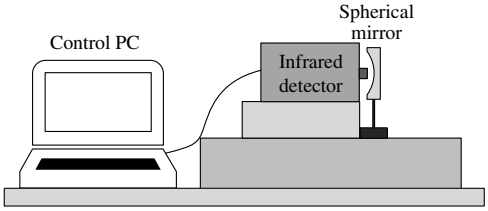

Fig. 7. Experimental setup for acquiring internal factors of the MWIR detector.

semidiameter of the entrance pupil of the MWIR detector is 5 mm, the length of the cryogenic dewar is 20 mm, and the half-length of the detector diagonal line is 6.147 mm. For typical infrared imaging systems, the rear working distance should be appropriate, not too close or too long. After consideration, the spherical mirror is placed 32 mm away from the IRFPA, which means L equals 32 mm. We get the radius range $14.415\ \text{mm} \le R \le 21.349\ \text{mm}$ on the basis of the theory described in Section 2. Considering the alignment error, we choose 18 mm as the radius; the height is 25 mm. The photo and parameter of the designed spherical mirror are displayed in detail in Fig. 6. The experimental setup is sketched in Fig. 7.

In order to acquire the internal factors of the MWIR detector, the integration time was set to 1 ms and 1.5 ms, and the detector output is 321 DN and 385 DN, respectively. According to Eqs. (14) and (15), the internal factors of the MWIR detector can be presented as $h_{\text{det1}} = 128\text{DN}$ and $h_{\text{det2}} = 193\text{DN}$.

C. Measurement Results and Analysis

Since the internal factors of the MWIR detector have been obtained, only a typical radiometric calibration is required to measure the internal stray radiation. The near-extended-source method is adopted to perform the calibration. Additionally, in order to ensure good performance, the whole experimental setup was put into a chamber with stable and controllable inside temperatures, as shown in Fig. 8. Experiments have implied that the inside temperature accuracy can be controlled within ± 0.5°C as long as the temperature is set in several minutes. An extra temperature sensor was put into the chamber to measure the actual temperature due to the temperature fluctuation inside the chamber.

The chamber temperature was set to 30°C, and the ambient temperatures last at least for 40 min to ensure that all parts

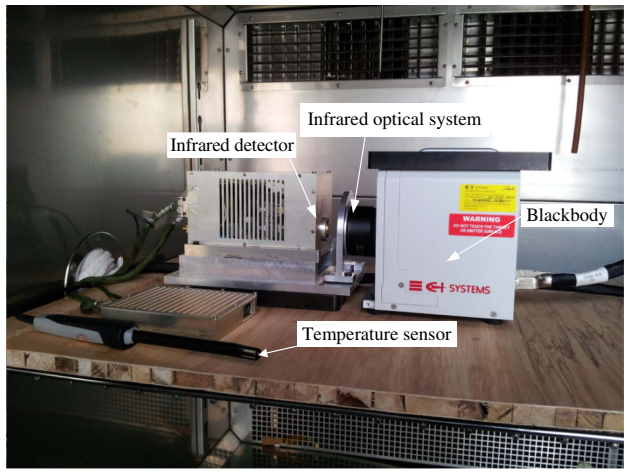

Fig. 8. Experimental setup for calibration.

of the infrared imaging system are at an equal temperature. The temperature of the reference source was set to 30°C, 40°C, 50°C, and 60°C, and the integration time was chosen as 0.2 ms, 0.5 ms, 0.8 ms, 1 ms, 1.2 ms, 1.5 ms, 1.8 ms, and 2 ms. According to Eq. (16), the output gray values caused by internal stray radiation can be obtained. The measurement results as a function of the integration time at 30°C are exhibited in Fig. 9. The curve of original data refers to the experimental values, and the curve of linear fitting is the linearly fitted result.

As we can see from Fig. 9, the output caused by internal stray radiation is in linear connection with the integration time, which is coincident with Eq. (16) and proves that the measurement results are valid. The quantitative relation between the output and the integration time is fitted as $h_{\text{stray}}(t, 30\text{°C}) = 353.983 \times t + 17.0295$. Theoretically, when the integration time is 0 ms, the output gray value caused by internal stray radiation should be zero as well. According to the fitted linear equation, the output is 17.0295 DN when the integration time is 0 ms, which agrees with the theoretical analysis.

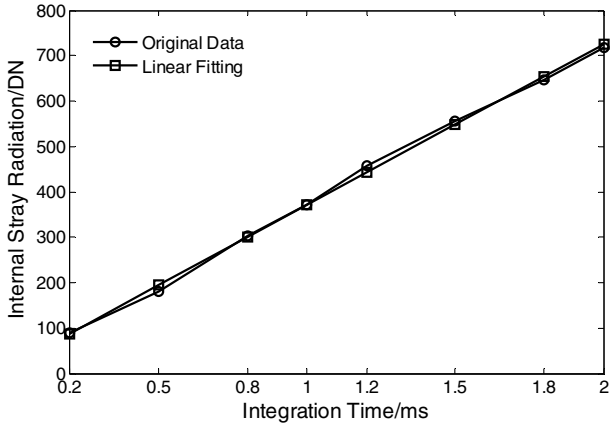

Fig. 9. Internal stray radiation as a function of integration time at 30°C.

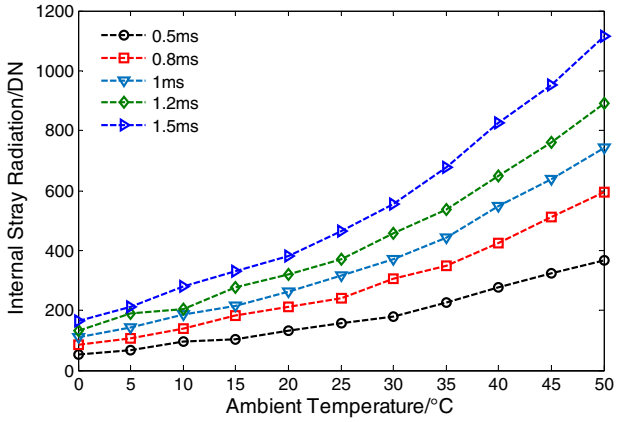

Fig. 10. Output gray values caused by internal stray radiation at several ambient temperatures and integration times.

To further validate the proposed theory at various ambient temperatures, the temperature inside the chamber was changed, varying from 0°C to 50°C, with 5°C as the interval. Similarly, each of the ambient temperatures last at least 40 min to make sure that all components of the infrared imaging system are at the same temperature, namely, the ambient temperature. The temperature of the blackbody was chosen as 30°C, 40°C, 50°C, and 60°C, and the integration time was set to 0.5 ms, 0.8 ms, 1 ms, 1.2 ms, and 1.5 ms. According to Eqs. (16) and (17), the internal stray radiation can be calculated. The measurement results are shown in Figs. 10 and 11.

As displayed in Fig. 10, with the ambient temperature rising, the output gray value caused by internal stray radiation grows rapidly and has a nonlinear relation to the ambient temperature. The curves are similar to the curve of blackbody radiation, which is consistent with theoretical analysis. Furthermore, the output gray values caused by internal stray radiation are in approximate proportion to the integration time under a certain ambient temperature, which proves that the measurement results are valid. It is illustrated in Fig. 11 that the flux originating from internal stray radiation at different

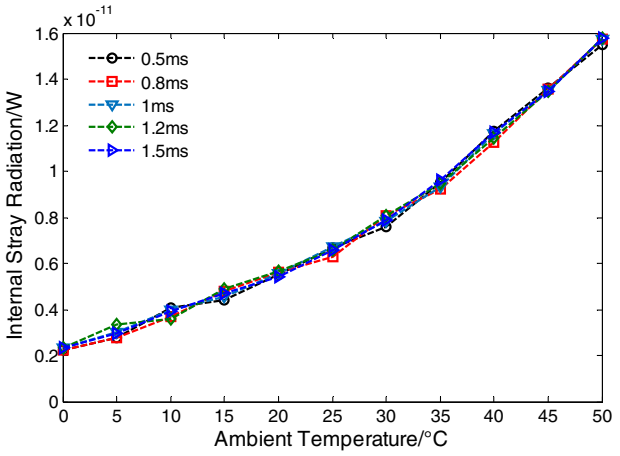

Fig. 11. Flux resulting from internal stray radiation at several ambient temperatures and integration times.

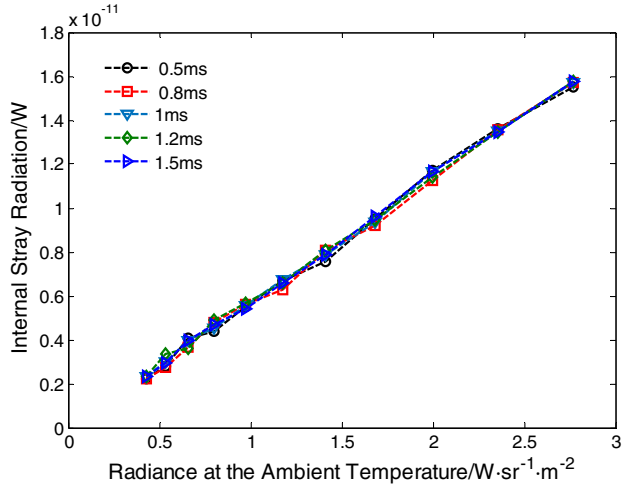

Fig. 12. Flux originating from internal stray radiation as a function of the radiance at the ambient temperature.

integration times agrees well with each other, which means the internal stray radiation flux is independent of the integration time. Figure 12 shows the internal stray radiation flux as a function of the radiance at the ambient temperature at several integration times.

Figure 12 illustrates that the internal stray radiation flux is approximately proportional to the radiance at the ambient temperature. The fitted lines are listed in Table 1. Table 1 indicates that the slopes of different lines are approximately equal, and the intercepts are nearly zero, which proves that the measurement results are convincing.

In theory, the output gray values caused by internal stray radiation should be in direct proportion to the integration time and the radiance of an ideal blackbody at the ambient temperature [25]. Figure 13 demonstrates that the measurement results coincide well with the theory, which further proves that the measurement results are correct. The fitted linear equations are listed in Table 2.

As shown in Table 2, the slopes of different lines are proportional to the integration time, which is consistent with the theoretical analysis. Theoretically, when the ambient temperature is 0 K, the internal stray radiation should be zero as well. Table 1 indicates that when the radiance at ambient temperature is zero, the intercepts of different lines are nearly zero, which accord well with the theory. As for the residual deviations, they are mainly caused by the detector output noise, which is about 20 DN.

Table 1. Fitted Equations Between Internal Stray Radiation Flux and Radiance at the Ambient Temperature

Integration Time/ms	Fitted Linear Equation
0.5	$\Phi_{stray}(0.5\,ms, L_{amb}) = 5.7460\times10^{-12}\times L_{amb} - 1.1754\times10^{-13}$
0.8	$\Phi_{stray}(0.8\,ms, L_{amb}) = 5.7337\times10^{-12}\times L_{amb} - 1.3792\times10^{-13}$
1	$\Phi_{stray}(1\,ms, L_{amb}) = 5.7132\times10^{-12}\times L_{amb} - 2.2551\times10^{-14}$
1.2	$\Phi_{stray}(1.2\,ms, L_{amb}) = 5.6569\times10^{-12}\times L_{amb} + 9.0720\times10^{-14}$
1.5	$\Phi_{stray}(1.5\,ms, L_{amb}) = 5.7357\times10^{-12}\times L_{amb} - 3.8254\times10^{-14}$

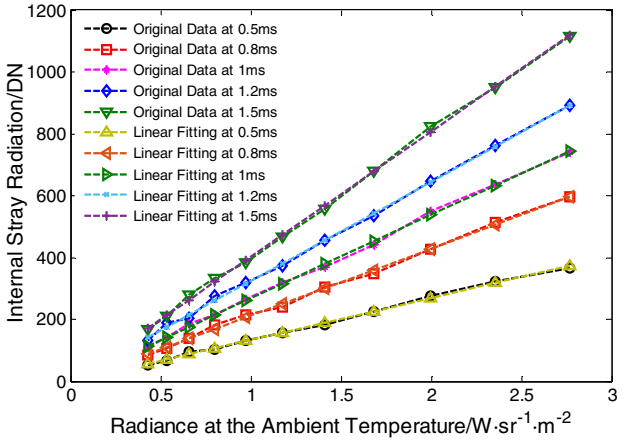

Fig. 13. Output gray values caused by internal stray radiation as a function of radiance at the ambient temperature.

Table 2. Linear Equations Between Internal Stray Radiation and Radiance at the Ambient Temperature

Integration Time/ms	Fitted Linear Equation
0.5	$h_{\text{stray}}(0.5\ \text{ms}, L_{\text{amb}}) = 135.9842 \times L_{\text{amb}} - 2.6386$
0.8	$h_{\text{stray}}(0.8\ \text{ms}, L_{\text{amb}}) = 216.7795 \times L_{\text{amb}} - 5.1327$
1	$h_{\text{stray}}(1\ \text{ms}, L_{\text{amb}}) = 269.5870 \times L_{\text{amb}} - 0.9968$
1.2	$h_{\text{stray}}(1.2\ \text{ms}, L_{\text{amb}}) = 320.1529 \times L_{\text{amb}} + 4.9322$
1.5	$h_{\text{stray}}(1.5\ \text{ms}, L_{\text{amb}}) = 405.1466 \times L_{\text{amb}} - 2.7432$

In summary, the measurement results are consistent with the theoretical analysis, which demonstrates that the theories introduced in this paper are valid, and the proposed method is applicable in practical applications. Besides, only a spherical mirror and a general radiometric calibration are required to achieve the measurement for internal stray radiation, which is simple to implement and has a low demand for experimental setup.

5. CONCLUSIONS

This paper has introduced a method based on radiometric calibration and a spherical mirror to measure the internal stray radiation of cryogenic infrared imaging systems. The validity of the method has been verified by experiments. On the basis of the principle that external thermal radiation cannot directly reach the infrared detector, the theory of spherical mirror design is presented. The calibration model is deduced considering the integration time. By positioning the spherical mirror in front of the infrared detector in the right place, the internal factors of the infrared detector can be obtained. Then, the internal stray radiation can be acquired by comparing the internal factors with the calibration result of the infrared imaging system at an integration time. Experiments have been performed in a chamber with controlled inside temperatures to validate the theories introduced in this paper. Experimental results indicate that the measurement results are in good agreement with the theoretical analysis, which demonstrates that the proposed theories and method are valid and can be used in engineering applications.

Only a spherical mirror and a typical radiometric calibration are required to achieve the internal stray radiation measurement, which has a low demand for experimental setup, and the proposed method can achieve accurate measurement for internal stray radiation. The measurement results can be used to evaluate whether the internal stray radiation suppression level meets the system requirement and to validate, as much as possible, the result of internal stray radiation analysis. What is more, the structure distortion or surface contamination can be detected in a timely way by monitoring the internal stray radiation in real time.

REFERENCES

1. S. M. Nejad, A. B. Madineh, and M. Nasiri, "Baffle design and evaluation of the effect of different parameters on its performance," Optik **124**, 6480–6484 (2013).
2. E. Fest, *Stray Light Analysis and Control* (SPIE, 2013).
3. J. L. Stauder, "Stray light design and analysis of the wide-field infrared explorer (WIRE)," Proc. SPIE **3122**, 35–44 (1997).
4. M. J. Sholl, F. S. Grochocki, J. C. Fleming, R. W. Besuner, P. Jelinsky, and M. L. Lampton, "Stray light design and analysis of the SNAP telescope," Proc. SPIE **6675**, 66750C (2007).
5. J. X. Niu, S. H. Shi, and R. K. Zhou, "Analysis to stray radiation of infrared detecting system," Proc. SPIE **8193**, 81931H (2011).
6. Y. Zhu, X. Zhang, T. Liu, Y. X. Wu, G. W. Shi, and L. Wang, "Internal and external stray radiation suppression for LWIR catadioptric telescope using non-sequential ray tracing," Infrared Phys. Technol. **71**, 163–170 (2015).
7. M. N. Akram, "Simulation and control of narcissus phenomenon using nonsequential ray tracing. I. Staring camera in 3–5 μm waveband," Appl. Opt. **49**, 964–975 (2010).
8. Y. Liu, X. Q. An, and Q. Wang, "Accurate and fast stray radiation calculation based on improved backward ray tracing," Appl. Opt. **52**, B1–B9 (2013).
9. X. L. Xia, Y. Shuai, and H. P. Tan, "Calculation techniques with the Monte Carlo method in stray radiation evaluation," J. Quant. Spectrosc. Radiat. Transfer **95**, 101–111 (2005).
10. C. R. Boshuizen, T. R. Bedding, M. L. Pfitzner, M. G. Grimminck, H. Kjeldsen, and A. G. Monger, "MONS space telescope, part 2: analysis of very high stray-light rejection," Opt. Eng. **47**, 013001 (2008).
11. A. V. Pravdivtsev and M. N. Akram, "Simulation and assessment of stray light effects in infrared cameras using non-sequential ray tracing," Infrared Phys. Technol. **60**, 306–311 (2013).
12. M. M. Talha, J. Chang, Y. Wang, T. Zhang, D. Cheng, and Z. Hui Sun, "Design, tolerancing and stray light analyses of a freeform HMD optical system," Optik **121**, 750–755 (2010).
13. K. S. Ellis, "Stray light characteristics of the large synoptic survey telescope (LSST)," Proc. SPIE **7427**, 742708 (2009).
14. F. Grochocki and J. Fleming, "Stray light testing of the OLI telescope," Proc. SPIE **7794**, 77940W (2010).
15. J. Fleming, F. Grochocki, T. Finch, S. Willis, and P. Kaptchen, "New stray light test facility and initial results," Proc. SPIE **7069**, 70690O (2008).
16. Q. F. Chen, Z. Ma, X. Y. Li, Z. H. Pang, L. Xu, and Z. H. Li, "Stray light measurement for point source transmittance of space optical systems," Proc. SPIE **9684**, 96842V (2016).
17. Q. J. Tian, S. T. Chang, Z. Li, F. Y. He, and Y. F. Qiao, "A method to measure internal stray radiation of cryogenic infrared imaging systems under various ambient temperatures," Infrared Phys. Technol. **81**, 1–6 (2017).
18. S. T. Chang, Z. Y. Sun, Y. Y. Zhang, and W. Zhu, "Internal stray radiation measurement for cooled infrared imaging systems," Acta Phys. Sin. **64**, 887–892 (2015).

19. Y. Lü, X. He, Z. H. Wei, Z. Y. Sun, and S. T. Chang, "Ambient temperature-independent dual-band mid-infrared radiation thermometry," Appl. Opt. **55**, 2169–2174 (2016).
20. M. Ochs, A. Schulz, and H. J. Bauer, "High dynamic range infrared thermography by pixelwise radiometric self calibration," Infrared Phys. Technol. **53**, 112–119 (2010).
21. T. Svensson, I. Renhorn, and P. Broberg, "Evaluation of a method to radiometric calibrate hot target image data by using simple reference sources close to ambient temperatures," Proc. SPIE **7662**, 76620X (2010).
22. Y. Té, P. Jeseck, I. Pépin, and C. Camy-Peyret, "A method to retrieve blackbody temperature errors in the two points radiometric calibration," Infrared Phys. Technol. **52**, 187–192 (2009).
23. B. G. Grant, *The Art of Radiometry* (SPIE, 2009).
24. Z. Y. Sun, S. T. Chang, and W. Zhu, "Radiometric calibration method for large aperture infrared system with broad dynamic range," Appl. Opt. **54**, 4659–4666 (2015).
25. S. T. Chang, Y. Y. Zhang, Z. Y. Sun, and M. Li, "Method to remove the effect of ambient temperature on radiometric calibration," Appl. Opt. **53**, 6274–6279 (2014).